Molecular Dynamics of Neutral and Protonated Ferrocene[#]

Michael Bühl* and Sonja Grigoleit

Max-Planck-Institut für Kohlenforschung, Kaiser-Wilhelm-Platz 1, D-45470 Mülheim an der Ruhr, Germany

Received October 1, 2004

Density-functional-based Car−Parrinello and Born−Oppenheimer molecular dynamics simulations are presented for ferrocene, $FeCp_2$, and its protonated form, $FeCp_2H^+$, in the gas phase, employing BP86 and B3LYP functionals. When the simulations for neutral $FeCp_2$ are started at 300 K from the eclipsed minimum, the system stays within that well for several picoseconds. When the simulations are started from the staggered transition state for Cp rotation, in contrast, free rotation of the Cp rings is observed with a rotational period of ca. 1 ps, in accord with the low barrier for rotation (ca. 1 kcal/mol at the BP86 level). $FeCp_2H^+$ is indicated to be fluxional on the picosecond time scale as well. The course of the dynamics depends strongly on the underlying quantum-chemical model. At the BP86 level, rotation of a Cp ring and large-amplitude motions of the proton are observed, and depending on details such as the particular basis set, structures with an essentially iron-bonded proton can prevail, or a significant population of structures with an additional agostic interaction to one of the Cp rings can occur. At the B3LYP level, the mobility of the proton is somewhat reduced, and agostic (or ring-protonated) structures are strongly preferred. Thermally averaged chemical shifts are computed from snapshots along the trajectory. ^1H and, in particular, ^{57}Fe chemical shifts in $FeCp_2H^+$ are sensitive to the location of the proton. The experimental $\delta(^{57}Fe)$ value is best reproduced in simulations that stay predominantly near the metal-protonated minimum, whereas the observed ^1H chemical shifts are better reconciled with an agostic structure. The same conclusion is drawn when zero-point corrections to equilibrium chemical shifts are evaluated using a perturbational approach. Molecular dynamics and chemical shifts of protonated ferrocene thus remain a challenge for approximate density functional theory.

Introduction

Fluxional behavior of molecules, that is, rapid intramolecular rearrangements, can be detected with a variety of experimental techniques, depending on the time scale of these processes. In most cases, observations can be rationalized computationally by locating the salient stationary points on an appropriate potential energy surface (PES) and calculating the reaction barriers involved. Interconversions with very low barriers in the 1−2 kcal/mol range occur on the picosecond time scale, requiring very fast spectroscopical techniques for direct observation. In such a case NMR spectroscopy, one of the most versatile analytical techniques available, is too slow, and only spectra averaged over the whole dynamic process can be obtained. When rearrangements involve degenerate minima with low symmetry, NMR spectra frequently display higher apparent symmetries.

Computations of NMR chemical shifts are a mature field by now,[1] and it has been recognized early on that calculated δ values can only agree with experiment when accurate molecular geometries are employed.[2] Very good results are usually obtained for static equilibrium chemical shifts using geometries optimized at a suitable level of ab initio or density functional theory (DFT), the latter being the method of choice for transition metal complexes.[3] When several possible candidates exist for a species giving rise to a particular NMR spectrum, certain isomers can usually be favored or excluded, based on the accord between computed and observed chemical shifts.[2]

The question is, how reliable and realistic are equilibrium chemical shifts computed for a static minimum when this is only a shallow valley on the PES and is involved in fast rearrangements? In other words, how sensitive are the theoretical δ values to the shape of the magnetic shielding hypersurface around the minimum and along the reaction path? This question can now be addressed by performing molecular dynamics simula-

[#] Dedicated to Prof. Dr. Paul v. R. Schleyer on the occasion of his 75th birthday.

* To whom correspondence should be addressed. Fax: Int. code + (0)208-306 2996. E-mail: buehl@mpi-muelheim.mpg.de.

(1) See for instance: (a) Helgaker, T.; Jaszunski, M.; Ruud, K. *Chem. Rev.* **1999**, *99*, 293−352. (b) Bühl, M.; Kaupp, M.; Malkin, V. G.; Malkina, O. L. *J. Comput. Chem.* **1999**, *20*, 91−105. (c) Kaupp, M., Bühl, M.; Malkin, V. G., Eds. *Calculation of NMR and ESR Parameters. Theory and Applications*; Wiley-VCH: Weinheim, 2004.

(2) See for instance: Bühl, M. In *Encyclopedia of Computational Chemistry*; Schleyer, P. v. R., Allinger, N. L., Kollman, P. A., Clark, T., Schaefer, H. F., Gasteiger, J., Schreiner, P. R., Eds.; Wiley: Chichester, 1998; pp 1835−1845.

(3) (a) Koch, W.; Holthausen, M. C. *A Chemist's Guide to Density Functional Theory*; Wiley-VCH: Weinheim, 2000. (b) See also the special issue of *Chem. Rev.* **2000**, *100,* (February 2000), pp 351−818 on Computational Transition Metal Chemistry.

10.1021/om049243g CCC: $30.25
Publication on Web 02/22/2005

tions and averaging the shieldings computed along the trajectory.[4,5]

When the system stays essentially within a sufficiently deep potential well during the time of the simulation, this procedure can model the effect of classical thermal averaging on the property of interest. When chemical shifts are particularly sensitive to geometrical parameters, the leading effects from thermal averaging of these parameters can be described qualitatively and can be traced back to the anharmonicity of the PES. We have recently used this methodology to assess thermal effects on transition metal chemical shifts,[6] which can be strongly dependent on the metal−ligand bond distances. While in individual cases this procedure has led to better agreement between calculated and observed chemical shifts, even with neglect of solvent effects in the simulations, no systematic improvement over a large set of metal complexes was found. Thus, these time-consuming simulations offer little in terms of increased accuracy of metal chemical shifts over those obtained from single, static equilibrium values. The same trends have been found when quantum-mechanical zero-point vibrational corrections, evaluated using a perturbational approach,[7] are applied to the equilibrium metal shifts.[6,8]

The situation may be different for fluxional molecules, however. Recent simulations studies have addressed this problem, following the evolution of nuclear shielding constants along "reactive" MD trajectories, that is, during molecular rearrangements. Systems studied so far comprise SF_4 during Berry pseudorotation (B3LYP level)[9] and $Sc_3N@C_{80}$ during rapid tumbling of the endohedral fragment inside the fullerene (semiempirical density functional tight-binding method).[10] We now present a similar study of ferrocene, $FeCp_2$, and its protonated form, $FeCp_2H^+$, calling special attention to rotational dynamics of the cyclopentadiene (Cp) units and proton migrations, and their manifestations in the averaged chemical shifts. The effect on the $\delta(^{57}Fe)$ value is of particular interest because, owing to their large chemical shift ranges,[11] transition metal nuclei can be much more sensitive to thermal and dynamic effects than the first-row nuclei.

As prototypical electrophilic attack, protonation of ferrocene has received considerable attention.[12−15] The protonation product is an intriguing organometallic species, which has defied structural characterization for a long time. Until the early 1990s the situation was that "while the proton affinity of ferrocene is well established, the site of protonation is not".[16] A number of theoretical studies have focused on the latter issue,[16−19] employing a variety of DFT methods and conventional ab initio techniques up to energy evaluations at a highly accurate coupled cluster level, CCSD(T).[17] From these studies, two minima have emerged as the most important ones, designated as metal-protonated (**2a**) and agostic (**2b**, see Scheme 1). Both are indicated to be quite similar in energy, with a slight preference for the agostic structure **2b**, both at the CCSD(T) and hybrid DFT levels.[17,12] In the NMR spectra of $FeCp_2H^+$, the added proton could be detected by its $\delta(^1H)$ value of −1.9 and −1.7 ppm in aqueous BF_3 and superacid,[12,13] respectively, that is, in an area characteristic for transition metal hydrides. Fluxional character of the molecule was indicated by the equivalence of all Cp resonances on the NMR time scale. On the basis of DFT (B3LYP) computed relative energies, interconversion barriers, and ^1H and ^{13}C chemical shifts, the experimental data were consistent with a mixture of **2a** and **2b**, with a barrier of at most 4.1 kcal/mol for migration of the proton along the equatorial perimeter of the $FeCp_2$ moiety.[13] According to recent B3LYP computations of the ^{57}Fe chemical shift, which has been known experimentally for some time,[14] metal-protonated **2a** seems to be the dominant constituent of the mixture.[20] We now present an explicit molecular dynamics study of this molecule and the consequences of its fluxionality on the NMR properties of interest, going beyond the static calculations reported so far.

Scheme 1

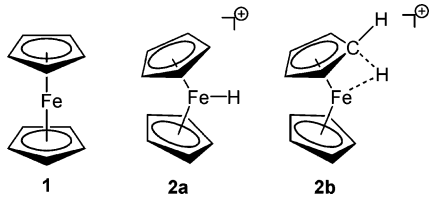

This paper is organized as follows: after a brief description of the computational methods, the results for neutral $FeCp_2$ are presented and discussed. Subsequently, the DFT methods to be used in the MD simulations are validated and applied to $FeCp_2H^+$. As it turns out, this molecule presents itself as another problem case for modern DFT methods, since the result can depend strongly on the theoretical level and since none of the simulations can reproduce both ^1H and ^{57}Fe chemical shifts at the same time.

(4) (a) Malkin, V. G.; Malkina, O. L.; Steinebrunner, G.; Huber, H. *Chem. Eur. J*. **1996**, *2*, 452−457. (b) Pfrommer, B. G.; Mauri, F.; Louie, S. G. *J. Am. Chem. Soc*. **2000**, *122*, 123−129. (c) Sebastiani, D.; Parrinello, M. *J. Phys. Chem. A* **2001**, *105*, 1951−1958.
(5) Bühl, M.; Parrinello, M. *Chem. Eur. J*. **2001**, *7*, 4487−4494.
(6) Bühl, M.; Grigoleit, S. *Chem. Eur. J*. **2004**, *10*, 5541−5552.
(7) (a) Ruud, K.; Åstrand, P.-O.; Taylor, P. R. *J. Chem. Phys*. **2000**, *112*, 2668−2683. (b) Ruud, K.; Åstrand, P.-O.; Taylor, P. R. *J. Am. Chem. Soc*. **2001**, *123*, 4826−4833. (c) Ruden, T.; Lutnæes, O. B.; Helgaker, T. *J. Chem. Phys*. **2003**, *118*, 9572.
(8) Bühl, M.; Imhof, P.; Repisky, M. *ChemPhysChem*. **2004**, *5*, 414−418.
(9) Pavone, M.; Barone, V.; Ciofini, I.; Adamo, C. *J. Chem. Phys*. **2004**, *120*, 9167−9174.
(10) Heine, T.; Vietze, K.; Seifert, G. *Magn. Reson. Chem*. **2004**, *42*, S199−S201.
(11) (a) von Philpsborn, W. *Chem. Soc. Rev*. **1999**, *28*, 95. (b) *Transition Metal Nuclear Magnetic Resonance*; Pregosin, P. S., Ed.; Elsevier: Amsterdam, 1991.
(12) ^1H NMR: (a) Curphy, T. J.; Santer, J. O.; Rosenblum, M.; Richards, J. H. *J. Am. Chem. Soc.* **1960**, *82*, 5249. See also: (b) Mueller-Westerhoff, U. T.; Haas, T. J.; Swigers, G. F.; Leipert, T. K. *J. Organomet. Chem.* **1994**, *472*, 229−246, and references therein.
(13) ^1H NMR: Karlsson, A.; Broo, A.; Ahlberg, P. *Can. J. Chem*. **1999**, *77*, 628−633.
(14) ^{57}Fe NMR: (a) Koridze, A. A.; Petrovskii, P. V.; Gubin, S. P.; Fedin, E. I. *J. Organomet. Chem.* **1975**, *93*, C26−C30. (b) Koridze, A. A.; Stakhova, N. M.; Petrovskii, P. V. *J. Organomet. Chem*. **1983**, *254*, 345−360.
(15) Gas-phase proton affinity: Meot-Ner, M. *J. Am. Chem. Soc*. **1989**, *111*, 2830−2834.
(16) McKee, M. L. *J. Am. Chem. Soc*. **1993**, *115*, 2818−2824.
(17) Mayor-López, M. J.; Lüthi, H. P.; Koch, H.; Morgantini, P. Y.; Weber, J. *J. Chem. Phys*. **2000**, *113*, 8009−8014.
(18) Irigoras, A.; Mercero, J. M.; Silanes, I.; Ugalde, J. M. *J. Am. Chem. Soc*. **2001**, *123*, 5040−5043.
(19) Borisov, Y. A.; Ustynyuk, N. A. *Russ. Chem. Bull. Int. Ed*. **2002**, *51*, 1900−1908.
(20) Wrackmeyer, B.; Tok, O. L.; Koridze, A. A. *Magn. Reson. Chem*. **2004**, *42*, 750−755.

Computational Details

Geometries were fully optimized in the given symmetry using Gaussian 98[21] and several gradient-corrected density functional combinations as implemented therein, namely, BP86,[22,23] BPW91,[22,24] BLYP,[22,25] and B3LYP.[25,26] These functionals usually perform well in typical applications in computational transition metal chemistry. A fine integration grid (75 radial shells with 302 angular points per shell) and the following basis sets have been used: AE1 denotes the Wachters basis (augmented by two diffuse p and one diffuse d sets) on Fe[27] and 6-31G* on the ligands;[28] in AE1(*) the extra proton is described by the 6-31G** basis. SVP[29] and TZVP[30] are the polarized split-valence basis sets from Ahlrichs and co-workers, addition of the two diffuse p and one diffuse d sets from Wachters and Hay[27] to Fe is labeled as SVP(+) and TZVP(+). In addition to these all-electron basis sets, relativistic effective core potentials (ECPs) with the corresponding valence basis sets were also employed on the metal, denoted LANL2DZ(d)[31] (together with Huzinaga double-ζ basis[32] on the ligands and one set of d-polarization functions on C with exponent 0.8), and ECP1[33] (no f-function on Fe, together with the 6-31G* basis on the ligands), the latter also in its nonrelativistic variant (denoted NR-ECP1). In general, the minimum character of the stationary points was verified by evaluation of the harmonic vibrational frequencies. In selected cases, geometries were also optimized at the RI-BP86 level as implemented in the TURBOMOLE program,[34] that is, making use of the resolution of identity and fitting of the density employing suitable auxiliary basis sets.[35]

Molecular dynamics simulations were performed using the Car−Parrinello scheme[36] as implemented in the CPMD program.[37] The BP86 combination of density functionals was used, together with norm-conserving Troullier−Martins pseudopotentials in the Kleinman−Bylander form.[38] Periodic boundary conditions were imposed using cubic supercells with box sizes of 11.5 Å. Kohn−Sham orbitals were expanded in plane waves up to a kinetic energy cutoff of 80 Ry. In the dynamical simulations a fictitious electronic mass of 600 au and a time step of 0.121 fs were used. To increase the simulation time step, hydrogen was substituted with deuterium. After an equilibration time of 0.5 ps at ca. 300 K, statistical averages and snapshots for the NMR calculations were collected from microcanonical runs 1 ps long. Equilibrium geometries for pristine complexes were obtained by optimizing the forces on all atoms with the CPMD program using the setup detailed above (denoted CP-opt). In selected cases additional optimizations were performed employing the gradient-corrected nonhybrid functional according to Hamprecht et al. (denoted HCTH).[39]

Additional Born−Oppenheimer MD simulations (denoted BOMD) were performed at the B3LYP/AE1 level, using Becke's hybrid functional as implemented in the TURBOMOLE program. MD simulations were performed using the ChemShell program[40] for NVE ensembles at ca. 300 K for 2.5 ps, with a time step of 0.5 fs. In these simulations, the 10 C−H distances in the Cp rings were frozen with the SHAKE algorithm. Data and snapshot sampling was started after the first 0.5 ps, which were taken for equilibration.

Magnetic shieldings σ were computed at the B3LYP level for equilibrium geometries and for snapshots taken from the MD simulations, employing GIAOs (gauge-including atomic orbitals)[41] and basis II, i.e., the augmented Wachters basis[27] on Fe and IGLO-basis II ,[42] which is essentially of polarized triple-ζ quality, on all other atoms. No periodic boundary conditions were imposed in the chemical shift calculations. Representative snapshots were taken every 20 fs. In most cases, the running averages of σ were reasonably well converged after 1−1.5 ps (40−60 snapshots),[5] with uncertainties of ca. ±50 ppm for $\sigma(^{57}\mathrm{Fe})$ and ca. ±0.1 ppm for $\sigma(^{13}\mathrm{C})$ and $\sigma(^{1}\mathrm{H})$, as estimated from the variations in the final values of the running average. Chemical shifts are reported relative to the usual standard molecules, $Fe(CO)_5$ for ^{57}Fe and TMS for ^{1}H and ^{13}C, which were optimized or simulated at the same respective level (σ values are given in Table 1). In selected cases, basis II′ was employed, which is the same as basis II, but uses only the DZ basis[42] on hydrogen. This level has been shown to perform very well for transition metal chemical shifts, including ^{57}Fe, where further enlargement of the basis set in the NMR part has afforded only minor changes in the computed values.[43,44]

Zero-point corrections were evaluated following the procedure from refs 7 and the stepsize parameters recommended in ref 8. Effective (vibrationally averaged) geometries r_{eff} were constructed at the BP86/AE1(*) and B3LYP/AE1(*) levels

(21) Frisch, M. J.; Trucks, G. W.; Schlegel, H. B.; Scuseria, G. E.; Robb, M. A.; Cheeseman, J. R.; Zakrzewski, V. G.; Montgomery, J. A.; Stratman, R. E.; Burant, J. C.; Dapprich, S.; Millam, J. M.; Daniels, A. D.; Kudin, K. N.; Strain, M. C.; Farkas, O.; Tomasi, J.; Barone, V.; Cossi, M.; Cammi, R.; Mennucci, B.; Pomelli, C.; Adamo, C.; Clifford, S.; Ochterski, J.; Petersson, G. A.; Ayala, P. Y.; Cui, Q.; Morokuma, K.; Malick, D. K.; Rabuck, A. D.; Raghavachari, K.; Foresman, J. B.; Cioslowski, J.; Ortiz, J. V.; Baboul, A. G.; Stefanov, B. B.; Liu, C.; Liashenko, A.; Piskorz, P.; Komaromi, I.; Gomperts, R.; Martin, R. L.; Fox, D. J.; Keith, T.; Al-Laham, M. A.; Peng, C. Y.; Nanayakkara, A.; Gonzalez, C.; Challacombe, M.; Gill, P. M. W.; Johnson, B. G.; Chen, W.; Wong, M. W.; Andres, J. L.; Gonzales, C.; Head-Gordon, M.; Replogle, E. S.; Pople, J. A. *Gaussian 98*; Gaussian, Inc.: Pittsburgh, PA, 1998.

(22) Becke, A. D. *Phys. Rev. A* **1988**, *38*, 3098−3100.

(23) (a) Perdew, J. P. *Phys. Rev. B* **1986**, *33*, 8822−8824. (b) Perdew, J. P. *Phys. Rev. B* **1986**, *34*, 7406.

(24) (a) Perdew, J. P., In *Electronic Structure of Solids*; Ziesche, P., Eischrig, H., Eds.; Akademie Verlag: Berlin, 1991. (b) Perdew, J. P.; Wang, Y. *Phys. Rev. B* **1992**, *45*, 13244−13249.

(25) Lee, C.; Yang, W.; Parr, R. G. *Phys. Rev. B* **1988**, *37*, 785−789.

(26) Becke, A. D. *J. Chem. Phys.* **1993**, *98*, 5648−5642.

(27) (a) Wachters, A. J. H. *J. Chem. Phys.* **1970**, *52*, 1033−1036. (b) Hay, P. J. *J. Chem. Phys.* **1977**, *66*, 4377−4384.

(28) (a) Hehre, W. J.; Ditchfield, R.; Pople, J. A. *J. Chem. Phys.* **1972**, *56*, 2257−2261. (b) Hariharan, P. C.; Pople, J. A. *Theor. Chim. Acta* **1973**, *28*, 213−222.

(29) Schäfer, A.; Horn, H.; Ahlrichs, R. *J. Chem. Phys*. **1992**, *97*, 2571−2577.

(30) Schäfer, A.; Huber, C.; Ahlrichs, R. *J. Chem. Phys*. **1994**, *100*, 5829−5835.

(31) Hay, P. J.; Wadt, W. R. *J. Chem. Phys.* **1985**, *82*, 270−283.

(32) Dunning, T. H.; Hay, P. J. In *Modern Theoretical Chemistry, Vol. 4*; Schaefer, H. F., Ed.; Plenum Press: New York 1977; pp 1−27.

(33) Dolg, M.; Wedig, U.; Stoll, H.; Preuss H. *J. Chem. Phys*. **1987**, *86*, 866.

(34) Ahlrichs, R.; Bär, M.; Häser, M.; Korn, H.; Kölmel, M. *Chem. Phys. Lett*. **1989**, *154*, 165.

(35) (a) Eichkorn, K.; Treutler, O.; Öhm, H.; Häser, M.; Ahlrichs, R. *Chem. Phys. Lett*. **1995**, *240*, 283. (b) Eichkorn, K.; Weigend, F.; Treutler, O.; Ahlrichs, R. *Theor. Chem. Acc.* **1997**, *97*, 119.

(36) Car, R.; Parrinello, M. *Phys. Rev. Lett*. **1985**, *55*, 2471−2474.

(37) Hutter, J.; Alavi, A.; Deutsch, T.; Bernasconi, M.; Goedecker, S.; Marx, D.; Tuckerman, M.; Parrinello, M. *CPMD* Version 3.3a; Max-Planck-Institut für Festkörperforschung and IBM Research Laboratory, 1995−1999.

(38) (a) Troullier, N.; Martins, J. L. *Phys. Rev. B* **1991**, *43*, 1993−2006. (b) Kleinman, L.; Bylander, D. M. *Phys. Rev. Lett*. **1982**, *48*, 1425−1428.

(39) Hamprecht, F. A.; Cohen, A. J.; Tozer, D. J., Handy, N. C. *J. Chem. Phys.* **1998**, *109*, 6264−6271.

(40) Sherwood, P.; deVries, A. H. *ChemShell−A Shell for Computational Chemistry*; CCLRC Daresbury Laboratory, 1999; see http://www.dl.ac.uk.

(41) (a) Ditchfield, R. *Mol. Phys*. **1974**, *27*, 789. (b) Wolinski, K.; Hinton, J. F.; Pulay, P. *J. Am. Chem. Soc*. **1990**, *112*, 8251. GIAO-DFT implementation: (c) Cheeseman, J. R.; Trucks, G. W.; Keith, T. A.; Frisch, M. J. *J. Chem. Phys.* **1996**, *104*, 5497.

(42) Kutzelnigg, W.; Fleischer, U.; Schindler, M. In *NMR Basic Principles and Progress Vol. 23*; Springer-Verlag: Berlin, 1990; pp 165−262.

(43) Bühl, M. *Chem. Phys. Lett.* **1997**, *267*, 251−257.

(44) The same was found in a few test calculations for the molecules of this study, where the use of a larger basis in the NMR part produced changes in the computed $\delta(^{57}\mathrm{Fe})$ values of just up to 20 ppm (using IGLO-III basis on the ligands, cf. ref 42, and a set of f-functions on iron, cf.: Bauschlicher, C. W.; Walch, S. P.; Partridge, H. *J. Chem. Phys*. **1982**, *76*, 1033).

Table 1. Magnetic Shielding Constants for Reference Compounds, Evaluated at the GIAO-B3LYP/II Level (in ppm)[a]

	$Fe(CO)_5$	TMS	
level of approximation	^{57}Fe	^{13}C	^{1}H
BP86/AE1	−2914	180.5	31.7
σ_{eff}	−2996	178.9	31.4
σ_0	−3012	178.4	31.4
BP86/CP-opt	−2919	181.9	31.8
CPMD σ_{av}	−3188	180.1	31.7
RI-BP86/SVP	−2733	179.5	31.5
BOMD σ_{av}	−3036	178.0	31.4
BP86/SVP	−2748	179.3	31.5
σ_{eff}	−2826	180.9	31.7
σ_0	−2841	181.9	32.5
BPW91	−2898	180.9	31.7
σ_{eff}	−2983	179.4	31.5
σ_0	−2999	178.8	31.4
BLYP/AE1	−3293	180.5	31.7
BLYP/ECP1	−3160	180.5	31.7
B3LYP/AE1	−3097	182.4	31.9
σ_0	−3200	180.9	31.7
σ_0	−3216	180.3	31.6
BOMD σ_{av}	−3488	179.7	31.8
B3LYP/TZVP	−2957	183.1	32.0

[a] Unless otherwise noted, equilibrium values (σ_e) are given; in some cases, values averaged over MD simulations (σ_{av}) or over zero-point motion (σ_{eff}, σ_0) are also given.

using the gradient technique (i.e., using analytical first derivatives in the numerical evaluation of the cubic force field)[8] and a step size of 0.25 au. Magnetic shieldings were evaluated at this point (denoted σ_{eff}) and vibrationally averaged, affording zero-point corrected value, σ_0. The shielding calculations were effected at the B3LYP/II level.

Results and Discussion

1. Ferrocene. Ferrocene, like the other isoelectronic (neutral or ionic) metallocene complexes, adopts an eclipsed conformation (see Scheme 1) in D_{5h} symmetry. The staggered D_{5d} form is the transition state for the rotation of the two Cp moieties with respect to each other and is 0.9 kcal/mol higher in energy at the BP86/CP-opt level, in excellent accord with estimates derived from gas-phase electron diffraction (GED).[45,46] Despite this low barrier, no spontaneous rotation was observed in a CPMD simulation starting from the minimum conformation. When, on the other hand, the simulation was started from the staggered D_{5d} form, essentially free rotation commenced immediately. This result is illustrated in Figure 1, which shows the evolution of an C−X−X−C angle (X = Cp midpoint) in both simulations. Apparently, when propagated from the transition state, the system follows the gradients pulling the two Cp rings toward eclipse. When the latter is reached, the two Cp rings carry sufficient momentum for the rotation to continue, eventually reaching and surpassing the next saddle point. In the simulation starting from the minimum, fairly large amplitudes are observed for this C−X−X−C angle (within ca. 10°, see dashed line in Figure 1), but not enough to reach the transition state

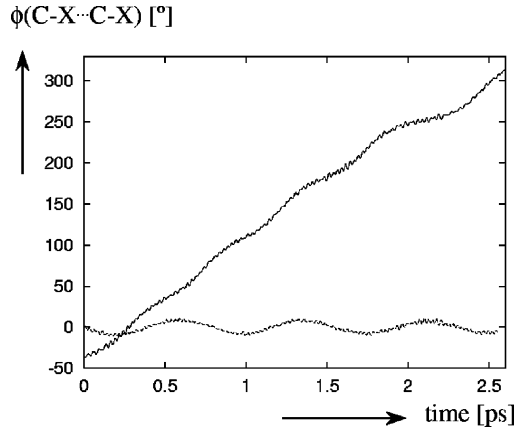

Figure 1. Evolution of the C−X−X−C angle (X = Cp midpoint) in BP86/CPMD simulations of ferrocene starting from the D_{5h} minimum (dashed) and the D_{5d} transition state for rotation (solid).

for rotation. A similar observation has been made for the rotational dynamics of the imidazole (Im) ligand in $VO(O_2)_2(Im)^-$.[47] In essence, this dependence of the course of the MD runs on the particular starting conditions implies that the simulations are not truly equilibrated. Distribution of the kinetic energy over all degrees of freedom at thermal equilibrium would probably require much longer simulation times. In principle, both simulations shown in Figure 1 should arrive at the same description of the rotational dynamics if continued long enough, or if collisions with other (solvent) molecules would occur, which would make the sampling more effective (see below).

The simulations for pristine $FeCp_2$ can be directly compared to results from GED, which have been used to derive the geometrical parameters of this molecule.[48] Overall, the experimental radial distribution (obtained at ca. 413 K) is well reproduced by those resulting from the two distinct CPMD simulations discussed above (see Figure 2). In general, the positions of the bands corresponding to bonding and nonbonding distances are well described computationally, in keeping with the finding that the molecular geometry of $FeCp_2$ is well reproduced with this particular density functional.[49] The observed bandwidths are somewhat larger than the simulated ones, at all probability due to the higher temperature in the GED experiment.

In the bonded and nonbonded region below 3.5 Å the curves from both simulations, that is, with and without free Cp rotation, practically coincide. The nonbonded distances in this area are those that involve C and H atoms within the same Cp ring. It is only for the distances involving C and/or H atoms in two different Cp rings that noticeable differences between both simulations arise. The corresponding region is shown at the bottom of Figure 2. Whereas broad, but distinct maxima for the C···C and C···H separations are discernible in the simulation that stays within the same potential well (solid curve), these have practically

(45) Derived barrier: 0.9 ± 0.3 kcal/mol. See: (a) Haaland, A.; Nilsson, J. E. *Chem. Commun*. **1986**, 88−89. (b) Haaland, A.; Nilsson, J. E. *Acta Chem. Scand*. **1968**, *22*, 2653−2670.

(46) Electrostatic arguments, specifically the induction energy of the metal in the potential field of the rings, have been put forward in order to rationalize the preference of the eclipsed over the staggered form of ferrocene: Carter, S.; Murrell, J. N. *J. Organomet. Chem*. **1980**, *192*, 399−408.

(47) Bühl, M.; Schurhammer, R.; Imhof, P. *J. Am. Chem. Soc*. **2004**, *126*, 3310−3320.

(48) Bohn, R. K.; Haaland, A. *J. Organomet. Chem*. **1966**, *5*, 470−476.

(49) (a) Bérces, A.; Ziegler T.; Fan, L. *J. Phys. Chem*. **1994**, *98*, 1584−1595. (b) Bühl, M.; Malkina, O. L.; Malkin, V. G. *Helv. Cim. Acta* **1996**, *79*, 742−754.

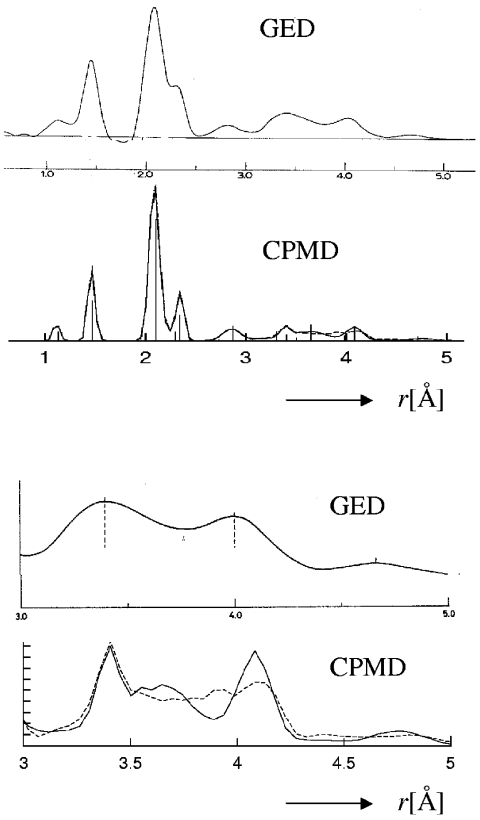

Figure 2. Radial distribution of gaseous ferrocene from experiment (GED, reprinted from ref 48 with permission) and CPMD simulations (sampled over 2 ps trajectories, solid: staying in one potential well; dashed: free Cp rotation): (top) whole spectrum, (bottom) nonbonded region above 3 Å.

completely smeared out into flat plateaus in the simulation that shows free Cp rotation (dashed line in Figure 2). Since such maxima are noticeable in the radial distributions from GED, the simulation with free rotation appears to fit less well to experiment than the one without.

To conclude from these data that no rotation would occur in ferrocene at room temperature and above would certainly be premature. However, these results do suggest that a model involving free and unhindered rotation, that is, with an essentially constant probability distribution function for the C−X−X−C angle, is unlikely, and that the system actually resides, on average, for a longer time in the regions close to the eclipsed minima than in those around the staggered transition structures. It is possible that a full quantum-dynamical description of the system (i.e., one taking also the quantum nature of the nuclei into account) could produce such a variable distribution function, in which case the rotational dynamics could be pictured more like a hopping mechanism between minima rather than a continuous, steady rotation. It is also possible that in the gas phase collisions with other molecules could induce such rotations, be they "continuous" or "hopping", but could also bring them to a halt again once started. In that case, the probability of finding the system close to a minimum would increase, even for a free-rotation model of the unperturbed system between collisions. Much more involved simulations, including suitable collision partners on a longer time scale, would be necessary to address this question in a more quantitative manner.[50]

Table 2. Computed (II′//GIAO-B3LYP) ^{13}C and ^{57}Fe Chemical Shifts for Ferrocene, Based on Equilibrium Structures and Averages over CPMD Trajectories (BP86 level)

	^{13}C		^{57}Fe	
level of approximation[a]	D_{5h}	D_{5d}	D_{5h}	D_{5d}
δ_e(CP-opt)	75.1	75.4	1524	1646
δ_{av}(CPMD)	74.5	74.9	1773	1869
δ *experiment*[d]	*69.2*		*1532*	

[a,c,d] See footnote in Table 1. [b] In parentheses: averaged, absolute magnetic shielding of the carbon atoms in **3**, which was used as primary standard.

What are the effects of dynamical averaging on the computed NMR chemical shifts? Equilibrium $\delta(^{57}Fe)$ and $\delta(^{13}C)$ values for minimum and transition state are given in Table 2, together with the corresponding averages over the single-well and free-rotation CPMD trajectories. All computed ^{13}C chemical shifts are quite similar; that is, they show little discrimination with respect to conformation and dynamics, and they are in good accord with experiment. In contrast, the $\delta(^{57}Fe)$ values display a noticeably larger sensitivity toward geometrical and thermal effects. On going from the equilibrium value of the D_{5h} minimum to that of the D_{5d} transition state, the iron nucleus is deshielded by ca. 100 ppm (compare CP-opt entries for D_{5h} and D_{5d} in Table 2). On going from the static D_{5h} minimum to the dynamic average of the "single-well" simulation, the ^{57}Fe nucleus is deshielded even more strongly, by ca. 200 ppm (compare CP-opt and CPMD entry for D_{5h} in Table 2). Since the equilibrium D_{5h} value is almost on top of experiment, dynamic averaging thus worsens the accord with the latter. The same has been found for a larger set of organoiron species, in particular for cyclopentadienyliron complexes.[6] On going from the dynamic average over the minimum region to that sampling the full rotation, a further deshielding of $\delta(^{57}Fe)$ is computed, by ca. 100 ppm (compare CPMD entries for D_{5h} and D_{5d} in Table 2). As with the radial distribution discussed above, the ^{57}Fe chemical shift of the D_{5h} minimum fits better to experiment than that of a free-rotation model, but in this case the difference is barely significant: The deviations from experiment, 241 and 337 ppm for single-well and free-rotation simulations, respectively, are close to the mean absolute deviation of CPMD-derived thermal averages obtained for the larger set of iron complexes (246 ppm).[6]

2. Protonated Ferrocene. 2.1. Dynamics. As an initial step to study the dynamics of $FeCp_2H^+$, we attempted to locate the relevant minima on the BP86 potential energy surface. Quite surprisingly, no agostic minimum **2b** was found in BP86/AE1 or in plane-wave-based CP/BP86 optimizations, which both afforded essentially the C_{2v}-symmetric metal-protonated form **2a**. Only when a set of polarization functions was added to the extra proton could a shallow minimum resembling an agostic structure be located at the BP86/AE1(*) level. It turned out that the structural and energetic characteristics of this minimum can be quite sensitive to the

(50) When the system starting from the D_{5d} structure is coupled to a thermostat set to 300 K (i.e., describing the NVT rather than the NVE ensemble), the same free rotation is observed.

Table 3. DFT-Optimized Geometrical and Parameters[a] (distances in Å, angles in deg) and Relative Energies ΔE (in kcal/mol)[b] for Protonated Ferrocene 2a and 2b (n.a.: not available)

	2a				2b						
level	Fe−X	X−Fe−X	Fe−H	H···C	Fe−X^1	Fe−X^2	X−Fe−X	Fe−H	H···C^1	H···C^2	ΔE
ΔE BP86/CP-opt	1.695	165.6	1.486	1.876			→ **2a**				–
BP86/AE1	1.686	165.7	1.504	1.894			→ **2a**				–
BP86/AE1(*)	1.685	166.2	1.497	1.880	1.673	1.681	168.5	1.569	1.403	2.264	-0.3
BP86/SVP	1.675	166.6	1.494	1.860	1.665	1.673	168.5	1.565	1.402	2.249	-0.1
BP86/SVP(+)	1.680	166.5	1.489	1.865	1.670	1.677	168.6	1.584	1.370	2.288	0.0
BPW91/6-311G[c]	1.692	166.6	1.507	n.a.	1.683	1.687	169.5	1.637	1.316	n.a.	0.1
BPW91/AE1	1.684	165.8	1.504	1.889	1.672	1.679	168.4	1.577	1.402	2.269	-0.5
BPW91/AE1(*)	1.682	166.3	1.496	1.874	1.671	1.679	168.6	1.577	1.380	2.278	-0.2
BLYP/LANL2DZ[d]	1.765	165.8	1.516	1.960	1.763	1.749	169.2	1.873	1.193	2.732	2.7
BLYP/LANL2DZ(d)	1.726	165.9	1.516	1.925	1.728	1.712	169.1	1.790	1.212	2.617	2.5
BLYP/ECP1	1.726	165.0	1.511	1.944	1.718	1.713	168.9	1.696	1.265	2.510	0.4
BLYP/NR-ECP1	1.733	165.2	1.514	1.947	1.729	1.720	168.9	1.724	1.239	2.557	1.2
BLYP/AE1	1.727	164.7	1.509	1.949	1.714	1.715	168.6	1.648	1.301	2.448	-0.6
BLYP/SVP(+)	1.720	165.6	1.503	1.921	1.710	1.713	168.8	1.639	1.303	2.432	0.1
BLYP/TZVP(+)	1.729	165.4	1.501	1.934	1.716	1.720	168.9	1.640	1.298	2.442	0.0
BLYP/CP-opt	1.740	164.7	1.499	1.961			→ **2a**				
HCTH/CP-opt	1.680	166.2	1.486	1.876	1.674	1.682	168.4	1.538	1.442	2.235	-0.8
B3LYP/6-311G[c]	1.720	166.5	1.491	n.a.	1.730	1.712	170.1	1.808	1.184	n.a.	3.8
B3LYP/6-311G(f)[e]	n.a.	n.a.	1.486	1.891	n.a.	n.a.	n.a.	1.785	1.19	n.a.	2.9
B3LYP/AE1	1.710	165.9	1.488	1.902	1.712	1.702	169.1	1.699	1.224	2.511	1.9
B3LYP/AE1(*)	1.708	166.4	1.481	1.886	1.711	1.703	169.2	1.682	1.229	2.491	2.4
B3LYP/SVP(+)	1.703	167.0	1.483	1.870	1.707	1.700	169.1	1.679	1.234	2.483	2.7
B3LYP/TZVP(+)	1.711	166.9	1.480	1.882	1.714	1.704	170.7	1.681	1.228	2.495	2.5
B3LYP/TZVP+G(3df,2p)[f]	n.a.	n.a	n.a	n.a	n.a	n.a	n.a	n.a	n.a	n.a	1.4
B3LYP/LANL2DZ(d)	1.708	167.2	1.496	1.873	1.731	1.701	169.3	1.819	1.180	2.639	5.7
B3LYP/ECP1	1.708	166.2	1.490	1.895	1.718	1.701	169.3	1.739	1.204	2.555	3.4

[a] X: midpoint of Cp ring (X1: ring closer to the extra proton). [b] Energy of **2a** relative to **2b** = 0.0. [c] From ref 17. [d] From ref 18; at that level, several other higher-lying minima (agostic or exo-protonated) are reported. [e] 6-31G basis on the ligands, from ref 12. [f] From ref 18.

density functional and to the basis set used in the optimizations. Some salient data are collected in Table 3. The structure of C_{2v}-symmetric iron-protonated **2a** is very similar at all levels, with Fe−H and H···C distances around 1.5 and 1.9 Å, respectively. That of the agostic isomer, if it can be located at all, is much more variable: The corresponding distances can vary within ca. 1.6−1.8 and 1.2−1.4 Å, respectively, depending on functional and basis set. The strongest interaction of the extra proton with one of the Cp rings is obtained with the B3LYP hybrid functional, which affords Fe−H and H···C distances of ca. 1.7−1.8 and 1.2 Å, respectively (see the last eight entries in Table 3). The results, in particular for B3LYP and BLYP functionals, also tend to be quite sensitive to the basis set and/or usage of an effective core potential (ECP), in which case the particular choice of the latter can also be important (compare, for instance, BLYP/LANL2DZ-(d) and BLYP/ECP1 entries in Table 3). In general, pure GGAs place **2a** and **2b** very close in energy, with a slight preference (typically a few tenths of a kcal/mol) for the former. B3LYP invariably predicts **2b** to be more stable than **2a**, by ca. 2−6 kcal/mol (Table 3). The same energetic sequence and a separation of about 2 kcal/mol was estimated from a series of coupled cluster calculations at the CCSD(T) level,[17] which is one of the most sophisticated wave function-based ab initio methods, and which has shown to afford reliable energetics of transition metal complexes.[51] The BLYP/ LANL2DZ-(d), B3LYP/AE1, and B3LYP/AE1(*) data in Table 3 are closest to this benchmark.

(51) For example: Frenking, G.; Antes, I.; Böhme, S.; Dapprich, M.; Ehlers, A. W.; Jonas, V.; Neuhaus, A.; Otto, M.; Stegmann, R.; Veldkamp, A.; Vyboishchikov, S. F. In *Reviews in Computational Chemistry, Vol. 8*; Lipkowitz, K. B., Boyd, D. B., Eds.; Wiley: New York, 1996; pp 63−144.

Since geometries and energies can be quite sensitive to the particular combination of density functionals, the MD simulations may take very different courses on the respective PESs. We will discuss three representative examples, namely, CPMD with the BP86 functional and BOMD at the B3LYP/AE1 and BP86/SVP levels. At the first of these, CPMD/BP86, the system is characterized by the presence of only one type of minimum, C_{2v}-symmetric **2a**. When the CPMD simulation is started from this minimum, the metal-bonded proton undergoes large-amplitude oscillations and immediately starts to move about the perimeter of the molecule. This ambulatory motion is illustrated by the evolution of one C−X−Fe−H dihedral angle (X = midpoint of the Cp ring) during the simulation. This angle is plotted in Figure 3a for two distinct trajectories starting from slightly different equilibrium geometries (one with essentially exact and one with more approximate C_{2v} symmetry). Hopping of the proton along the perimeter is fast on the picosecond time scale, and completion of a full cycle (which would correspond to dihedral angles spanning 360°) is expected to take just a few picoseconds, based on extrapolation of the curves in Figure 3a.

Concomitant with proton migration, the two Cp rings are rotating relative to each other. This process is monitored in Figure 3b via the C−X···X−C dihedral angle involving C atoms and midpoints of the two Cp rings. Unlike in the case of neutral ferrocene discussed above, rotation in the protonated form commences immediately, even if started from the minimum. We note in passing that the course of the two MD runs analyzed in Figure 3 is qualitatively very similar, suggesting that—even if they do not represent statistically significant sampling—the trajectories are not

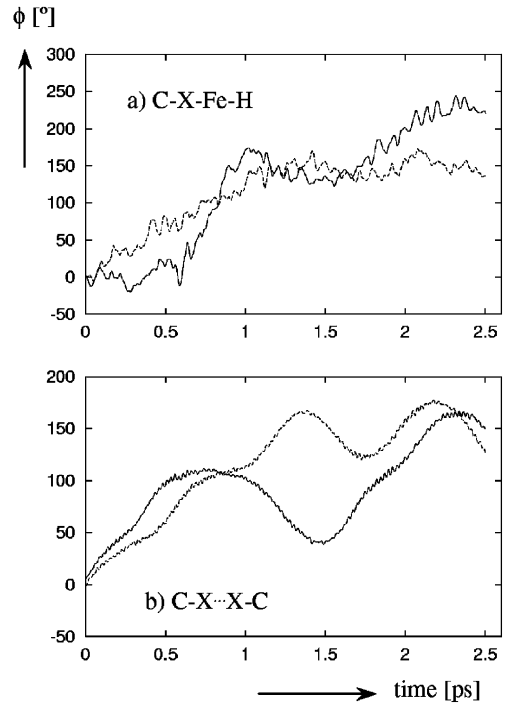

Figure 3. Evolution of dihedral angles in CPMD/BP86 simulations starting from **2a**: (a) C−X−Fe−H, (b) C−X···X−C (X: midpoint of Cp ring); in both cases data from two different trajectories are shown (solid and dashed lines correspond to simulations starting from minimized structures with approximate and exact C_{2v} symmetry).

artifacts of singular events, but should be typical for the dynamic processes on this PES.

Subsequently, two BOMD/B3LYP/AE1 simulations were started from each of the minima **2a** and **2b** located at that level, at which the CCSD(T) relative energies are best reproduced. The system starting from the lower minimum **2b** essentially stayed within the same potential well for the whole time of the simulation. No rotation of the Cp rings or hopping of the proton was observed. This result is illustrated in Figure 4a, which shows that the distances of the extra proton to the nearest C atoms of each ring just oscillate around their respective equilibrium positions (ca. 1.2 and 2.5 Å, see also the B3LYP/AE1 entry in Table 3).

When the simulation is started from the higher-lying minimum **2a**, the proton is more mobile: within about 0.15 ps it forms the agostic interaction with one C atom characteristic for **2b**. The proton does not stay there for the remainder of the simulation, but is reversibly transferred to an "opposing" C atom in the other Cp ring. Three such "back-and-forth" hopping events have been observed in the total simulation time of 2.5 ps (including equilibration). The first such event started at ca. 0.3 ps and proceeded via the intermediate occurrence of a structure resembling **2a**, which remained stable for ca. 0.2 ps before the proton was passed on to the other Cp ring. The second proton transfer occurred at ca. 1.3 ps; it was completed within 0.1 ps and was immediately followed by the reversion of this process, that is, the return of the proton to its position before the second jump, which again took little more than 0.1 ps (see the evolution of the C···H distances in Figure 4b). In the latter two jumps the proton passed continuously over the symmetrical position between the rings, and no noticeable intermediacy of **2a** was observed.

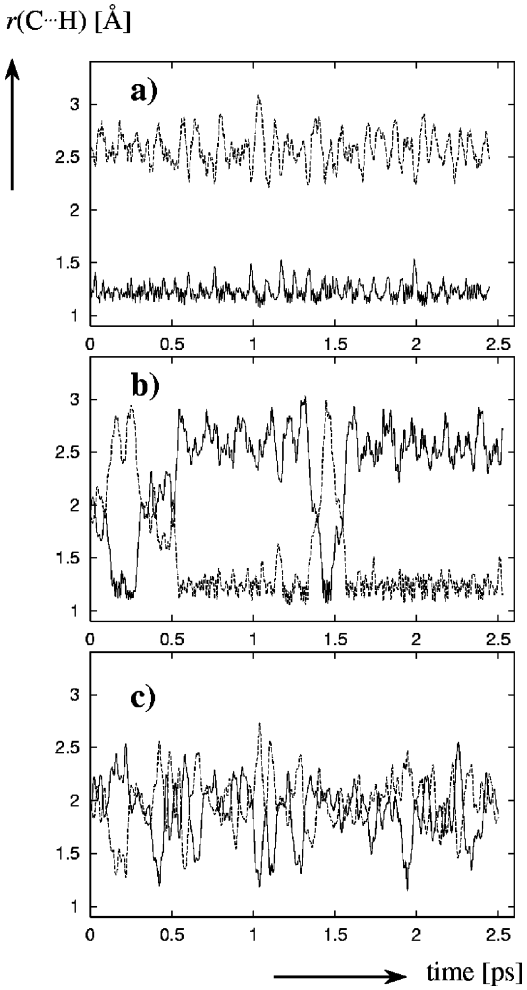

Figure 4. Evolution of the distances between the extra proton and the nearest C atom of each Cp ring: (a) BOMD/B3LYP starting from **2b**; (b) BOMD/B3LYP starting from **2a**; (c) CPMD/BP86 starting from **2a**.

For comparison, the corresponding C···H distances from a CPMD/BP86 simulation are included in Figure 4c. In this case, the proton oscillates around the symmetrical position characteristic for **2a** (with an average C···H separation somewhat larger than the equilibrium value of ca. 1.88 Å, Table 3) and occasionally approaches a C atom to distances below 1.3 Å, but stays there only for a very short time before it is deflected back toward the pseudo-symmetry axis.

During the BOMD/B3LYP simulation starting from **2a**, the Cp rings rotated relative to each other, but somewhat slower than in the CPMD/BP86 simulations (compare the variation of the dihedral angles in Figures 5 and 3b). The mobility of the proton around the perimeter of the complex is also less pronounced in the BOMD/B3LYP than in the CPMD/BP86 simulations. The solid line in Figure 4b stems from the same pair of atoms during the whole simulation time, whereas the dashed line involves transfer of the proton from one C atom of the Cp ring to an adjacent one, occurring about halfway through the trajectory. The singularity of this event notwithstanding, it is to be expected that proton migration is fast enough to scramble all Cp C and H atoms on the NMR time scale.

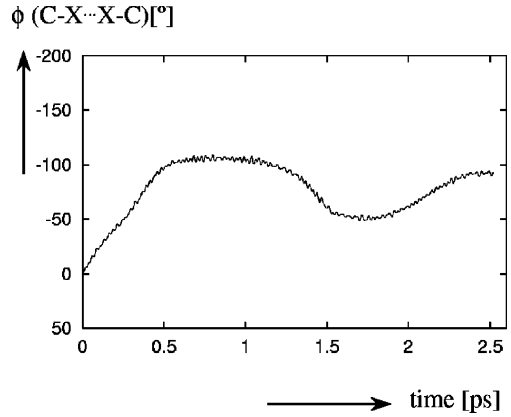

Figure 5. Evolution of the C−X···X−C dihedral angle in a BOMD/B3LYP simulation starting from **2a** (X: midpoint of Cp ring).

The differences between the two BOMD/B3LYP trajectories are consistent with the energetics on the PES: the barrier between **2a** and **2b** is relatively small, and a transition state connecting both has been reported to be only 0.4 kcal/mol above **2a** at the B3LYP/6311G(f) level.[12] Such a low barrier is easily overcome, so that **2a** readily collapses to the more stable minimum **2b**. To reach the transition state from the latter requires 3.3 kcal/mol at the same level. While still low enough to allow for very rapid processes (especially on the NMR time scale), this barrier is apparently high enough to require much longer simulation times than just 2 ps for reversible crossings. That two such reversible rearrangements are encountered in the simulation starting from **2a** is probably related to the fact that the potential energy released upon the formation of **2b** from **2a** results in a slightly higher average temperature (kinetic energy) in the microcanonical ensemble (ca. 15 K above the average temperature in the simulation starting from **2b**).

Finally, we performed MD simulations at a level at which a more even distribution of both isomers was to be expected. From the data in Table 3, BP86 and BLYP functionals together with the Ahlrichs SVP- and TZVP-type basis sets emerged as the most promising candidates in that respect, since **2a** and **2b** are virtually isoenergetic with any of the resulting combinations. Because of the better performance of BP86 over BLYP for the geometry of ferrocene, which is also reflected in a better description of the ^{57}Fe chemical shift when a BP86 geometry is employed (see below), RI-BP86/SVP was chosen eventually. Salient geometrical parameters, obtained from simulations starting from both minima, are monitored in Figure 6.

The resulting trajectories exhibit the same overall characteristics as those of the CPMD/BP86 simulations discussed above, namely, rapid proton migration, both between rings and around the perimeter, and Cp rotation. Agostic structures are much more prominent in the RI-BP86/SVP than in the CPMD/BP86 trajectories, however: C···H contacts below ca. 1.4 Å (associated with such agostic structures) are more frequent in Figures 6a,b than in Figure 4c. In addition, individual such C···H contacts can survive up to ca. 150 fs at the RI-BP86/SCP level. Thus, as expected, significant populations of metal- and ring-protonated structures are found at that level.

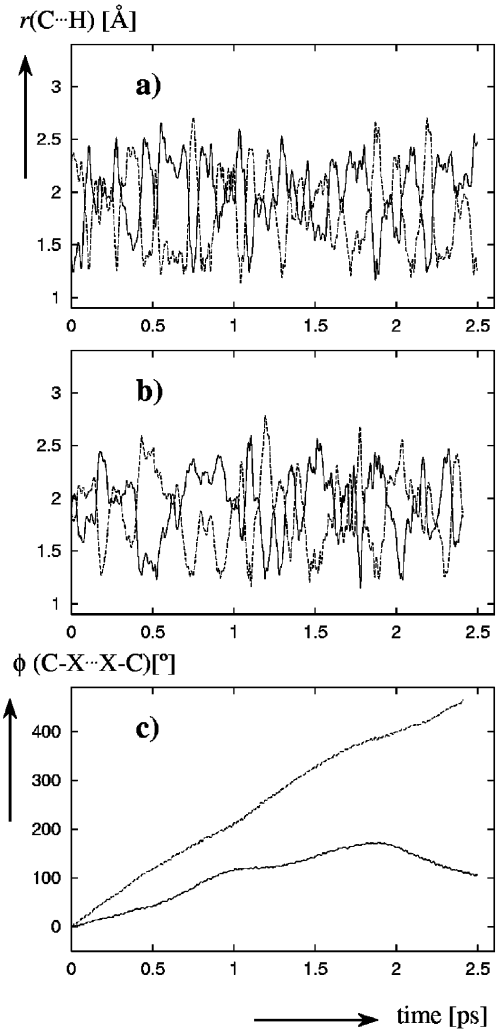

Figure 6. Evolution of geometrical parameters in BOMD/RI-BP86/SVP simulations: (a) distances between the extra proton and the nearest C atom of each Cp ring, simulation starting from **2b**; (b) same as (a), but starting from **2a**; (c) C−X···X−C dihedral angle starting from **2b** (solid line) and starting from **2a** (dashed).

The simulation starting from symmetric **2a** is characterized by a somewhat faster Cp rotation than noted so far for **1** or **2** (see dashed line in Figure 6c, note the different scale with respect to Figures 1, 3b, and 5). Apart from that detail, the two RI-BP86/SVP trajectories starting from **2a** or **2b** appear to follow qualitatively very similar courses.

In summary, the characteristics emerging from the CPMD/BP86, BOMD/B3LYP, and BOMD/RI-BP86/SVP simulations are fully consistent with the stationary points and their relative energies on the respective PESs. At the former level, the only minimum is symmetrical **2a**, whereas with B3LYP/AE1, the agostic minimum **2b** is more stable, and **2a** is not significantly populated. A more balanced distribution of metal- and ring-protonated structures is observed at the RI-BP86/SVP level, where **2a** and **2b** are almost degenerate.

2.2. Chemical Shifts. The chemical shifts of **1** and **2**, computed at several representative levels of theory, are collected in Table 4. When looking at the equilibrium values (in normal face), it is apparent that the results can be very dependent on the geometry that is employed. For instance, the experimental $\delta(^{57}\text{Fe})$ value of

Table 4. Computed Chemical Shifts (GIAO-B3LYP/II level) for Neutral and Protonated Ferrocene[a]

	1[b]		**2a**				**2b**			
level of approximation	^{57}Fe	^{13}C	^{57}Fe	^{13}C[c]	^{1}H(Fe)	^{1}H(Cp)[c]	^{57}Fe	^{13}C[c]	^{1}H(Fe)	^{1}H(Cp)[c]
BP86/AE1(*)	1481	73.9	132	84.7	5.5	4.9	715	81.6	−1.0	4.8
δ_{eff}	*1574*	*73.3*	*221*	*84.0*	*5.7*	*4.7*	*107*	*84.0*	*5.4*	*4.8*
δ_0	*1578*	*73.1*	*235*	*83.7*	*5.6*	*4.8*	*116*	*83.7*	*5.3*	*4.9*
BP86/CP-opt	1524	74.1	302	86.3	5.7	5.0			→ **2a**	
CPMD δ_{av}	*1773*	*74.5*	*529*	*84.7*	*5.7*	*5.0*			→ **2a**	
RI-BP86/SVP	1439	73.5	154	83.9	4.8	4.8	746	80.7	−1.6	4.7
BOMD δ_{av}	*1607*	*73.4*	*617*	*82.5*	*2.8*	*4.8*	*616*	*82.5*	*2.9*	*4.8*
BP86/SVP	1449	73.6	139	83.7	4.8	4.8	702	80.8	−1.2	4.7
δ_{eff}	*1534*	*75.8*	*227*	*86.0*	*5.4*	*5.1*	*175*	*85.8*	*5.0*	*5.2*
δ_0	*1540*	*75.5*	*240*	*87.2*	*6.2*	*6.0*	*189*	*87.0*	*5.8*	*6.0*
BLYP/AE1	2046	73.5	562	86.1	8.5	5.0	1748	90.3	−3.6	4.8
BLYP/ECP1	2214	73.5	703	86.0	8.5	5.0	2319	90.0	−5.3	4.7
B3LYP/6-311G(f)[d]	n.a.	n.a.	n.a	68.1	3.1	5.2	n.a.	62.4	−6.4	5.1
B3LYP/AE1(*)	2197	73.6	328	84.9	7.4	4.9	2161	79.8	−6.3	4.7
δ_{eff}	*2310*	*71.9*	*405*	*84.0*	*7.5*	*4.8*	*2038*	*79.3*	*−4.9*	*4.6*
δ_0	*2317*	*71.7*	*408*	*83.8*	*7.6*	*4.8*	*2055*	*79.1*	*−4.8*	*4.6*
B3LYP/AE1	2197	73.6	357	85.1	7.5	4.9	2361	80.2	−6.1	4.7
BOMD δ_{av}	*2333*	*71.2*	*2094*	*80.2*	*−2.1*	*4.7*	*2790*	*79.1*	*−5.5*	*4.7*
B3LYP/TZVP(+)	2420	72.6	512	84.8	7.6	4.9	2379	79.8	−6.2	4.7
experiment	***1532***	***69.2***	***429***	***77.1***	***−1.7***	***5.1***	***429***	***77.1***	***−1.7***	***5.1***

[a] In normal face: equilibrium values, δ_e; in italics: values averaged over MD trajectories (δ_{av}) or zero-point motion (δ_{eff}, δ_0). [b] B3LYP/II′ level. [c] Averaged values. [d] Shifts calculated at the GIAO-B3LYP/6-311G(f,d,p) level, from ref 12.

1 is best reproduced with BP86-derived geometries, whereas BLYP- or B3LYP-optimized structures produce much too high ^{57}Fe chemical shifts (with errors exceeding 500 ppm). These findings can be rationalized by the notable overestimation of the iron−ligand distances with the latter two functionals: using the AE1 basis, the optimized Fe−C separations are ca. 2.08 Å with BLYP and B3LYP, compared to 2.054 Å obtained with BP86[49b] and 2.056 Å observed in the gas phase (GED[48]). Together with the computed shielding/bond length derivative of −232 ppm/pm,[52] a spurious bond length increase by 2−3 pm (as in the BLYP and B3LYP geometries) may well result in errors in $\delta(^{57}\text{Fe})$ by several hundred ppm. The ^{13}C chemical shift, in contrast, is much less geometry-dependent and is close to ca. 74 ppm at all levels considered, in reasonable accord with experiment.[53]

On going from **1** to metal-protonated **2a**, the ^{57}Fe chemical shift is drastically reduced, in apparent qualitative agreement with experiment. The computed $\delta(^{57}\text{Fe})$ data, ca. 100−700 ppm, bracket the experimental value at ca. 400 ppm (Table 4). From this accordance one could be tempted to conclude that it is this C_{2v} structure that is observed in the NMR experiments. However, none of the geometries employed produce a ^{1}H resonance of the metal-bonded proton that would be even remotely close to the observed "hydridic" value at $\delta = -1.7$,[12] that is, shifted upfield from TMS. All computed values are higher than +3 ppm, and most are higher than ca. +5 ppm (see ^{1}H(Fe) data for **2a** in Table 4).

In contrast, "hydridic shifts"[54] are computed for the extra proton in all agostic minima (see normal-face ^{1}H(Fe) entries for **2b** in Table 4). This observation, namely, that the proton resonance can only be reconciled with an agostic structure, was already made in ref 12, where it was noted that the $\delta(^{1}\text{H})$ values obtained at GIAO-B3LYP/6-311G(f,d,p)//B3LYP/6-311G(f) fit very well to experiment when averaged over both **2a** and **2b**. There are two problems with such an implicit assignment, however: First, the extent of the "hydridic shift" in **2b** is very sensitive to the underlying geometry and can vary between ca. −1 ppm (BP86 minima) and −6 ppm (B3LYP geometries), quite a substantial span for $\delta(^{1}\text{H})$. Second, the ^{57}Fe resonance is also highly variable and can assume values between ca. 700 ppm and well above 2000 ppm. In particular the values for the B3LYP/AE1 and B3LYP/AE1(*) geometries, ca. 2100 ppm,[55] deviate significantly from experiment, $\delta = 429$.

The mean C and H resonances from the Cp ligand are of little diagnostic value: Since they are dominated by nuclei not involved in interactions with the extra proton, they differ only little between **2a** and **2b**. Of all the static equilibrium data in Table 4, those computed for **2b** in the BP86/AE1(*) geometry fit best to experiment, with absolute deviations of 286 and 0.6 ppm for ^{57}Fe and ^{1}H(Fe) chemical shifts, respectively.

As mentioned in the Introduction, however, the computation of static equilibrium chemical shifts may not be sufficient in this case, where, due to the shallow PES and low barriers, the nuclei can sample much larger areas of the PES. When the chemical shifts are averaged over the CPMD/BP86 trajectory, where only areas around one type of minimum are sampled (**2a**), only small to moderate changes with respect to the equilibrium values are found: The ^{57}Fe nucleus is deshielded by slightly more than 200 ppm due to thermal motion, much the same as the metal center in ferrocene itself (compare BP86/CP-opt and CPMD entries in Table 4). The chemical shift of the iron-bonded proton is remarkably unaffected by thermal averaging, despite the large-amplitude motions documented in

(52) That is, the Fe nucleus is deshielded by 232 ppm upon increase of all Fe−C distances by 1 pm; value taken from ref 6.

(53) Chemical shifts of ligands in the coordination sphere of transition metals are usually well described with DFT methods, see e.g. ref 1b and: M. Kaupp, V. G. Malkin, O. L. Malkina, D. R. Salahub. *Chem. Phys. Lett*. **1995**, *235*, 382.

(54) The upfield ^{1}H resonances in transition metal hydrides are not a consequence of negative charge accumulated on these protons, but arise rather from the anisotropy of the (paratropic) current loops at the nearby metal: Ruiz-Morales, Y.; Schreckenbach, G.; Ziegler, T. *Organometallics* **1996**, *15*, 3920−3923.

(55) Unfortunately, the value for the B3LYP/6-311G(f) geometry was not reported in ref 12.

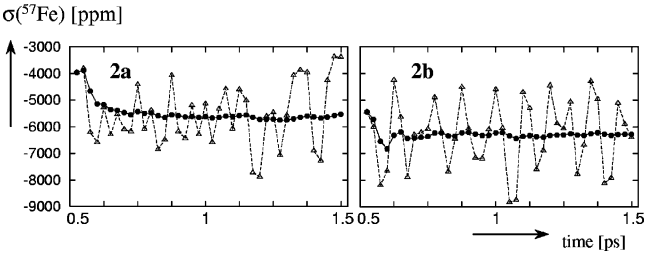

Figure 7. Evolution of the ^{57}Fe magnetic shielding constants from individual snapshots (open triangles) and the corresponding running averages (filled squares) in B3LYP BOMD simulations starting from **2a** (left) and **2b** (right).

Figure 4c. This mobility is reflected in large fluctuations of the ^{1}H shifts along the trajectory, and those snapshots that resemble agostic structures are indeed characterized by noticeable "hydridic" shifts of the extra proton (up to $\delta = -4.3$). However, such pronounced agostic structures are rare, too rare to affect the mean ^{1}H(Fe) chemical shift significantly.

Larger dynamical effects on the chemical shifts are found for the BOMD/B3LYP simulations. When the δ values are averaged over the trajectory starting from **2b**, which stayed in the same potential well all the time, a slight deshielding is predicted for ^{1}H(Fe), from $\delta = -6.1$ (equilibrium value) to $\delta = -5.5$ (dynamic average, compare B3LYP/AE1 and BOMD entries in Table 4). The ^{57}Fe nucleus is strongly deshielded, by more than 400 ppm, which further worsens the agreement with experiment.

At the beginning of snapshot sampling (after 0.5 ps), the simulation starting from **2a** had already produced agostic structures resembling **2b** (see Figure 4b). As a consequence, the dynamic averages over the remainder of the trajectory (which we will continue to identify with the label **2a**) afford signatures qualitatively similar to those obtained from the trajectory from **2b** itself, namely, a strongly deshielded metal and a "hydridic" proton resonance (δ values ca. 2100 and -2 ppm, respectively, see Table 4). Despite the overall similarity of both simulations (i.e., whether starting from **2a** or **2b**), the quantitative thermal NMR averages are notably different, with offsets of ca. 700 and 3 ppm for ^{57}Fe and ^{1}H(Fe) shifts, respectively (compare B3LYP BOMD entries for **2a** and **2b** in Table 4). That the average ^{57}Fe shielding constants that are used to calculate the δ values are reasonably well converged is demonstrated in Figure 7: While the shieldings of individual snapshots can vary by several thousands of ppm, the corresponding running averages (filled circles in Figure 7) show no clear drift in the final part of each trajectory.[56] Eventually, however, the long-time averages should gradually approach each other and would probably converge to an intermediate value.[57]

The strong deshielding of the ^{57}Fe nucleus upon dynamic averaging can be rationalized upon inspection of those snapshots with very low shielding constants (high chemical shifts): these are characterized by very long Fe−H distances (sometimes exceeding 2 Å) and short C−H bonds. In the limiting case of a full CH σ-bond and no interaction between Fe and H (i.e., for an ideal exo-protonated form), the resulting neutral cyclopentadiene ligand would just act as a four-electron donor, producing a 16-electron complex. As a model for such a species, we have optimized the open 1,3-butadiene complex $FeCp(\eta^4\text{-}C_4H_6)^+$, for which a $\delta(^{57}\text{Fe})$ value of 8953 ppm is obtained at the GIAO-B3LYPII′//BP86/AE1 level. This 16e species has a very low-lying unoccupied MO with large d(Fe) character, consistent with large paramagnetic contributions to the shielding constant and, thus, to the huge deshielding of the metal. When converted to δ using the B3LYP BOMD standard value from Table 1, the lowest shielding encountered for any snapshot in Figure 7 (at about 1.05 ps in **2b**) corresponds to $\delta \approx 5300$, suggesting that, even though not fully reached, this limiting situation of a 16e complex can be approached to some extent.

From the B3LYP MD results it can be concluded that, whether starting from **2a** or **2b**, it is mainly areas around structures resembling **2b** that are sampled, and the resulting thermally averaged chemical shifts are qualitatively similar to the δ_e values of that isomer. This finding is again consistent with the relative energies of the stationary points discussed above, namely, that **2b** is more stable than **2a** by ca. 2 kcal/mol (corresponding to a ca. 97:3 equilibrium mixture at room temperature) and that barriers between them are low. While the ^{1}H resonance of the extra proton modeled with this dynamic approach is in qualitative accord with experiment, the averaged Fe chemical shift is not. Part of this problem may be related to the fact that B3LYP is plagued by problems with the $FeCp_2$ geometry.

In contrast to the CPMD/BP86 and BOMD/B3LYP simulations discussed so far, which sample predominantly species corresponding to **2a** and **2b**, respectively, a more balanced population between both species is found at the RI-BP86/SVP level. This situation is reflected in the averaged chemical shifts: Whether starting from **2a** or from **2b**, essentially the same mean values are obtained for the respective nuclei listed in Table 4 (see BOMD values in italics), and these values are between those of the static minima **2a** and **2b** (see δ_e values in normal face). In fact, if a 50:50 mixture of both is assumed (consistent with their equal energies) and the δ_e values are averaged accordingly, chemical shifts quite close to the δ_{av} values from the MD simulations are obtained. For $\delta(^{57}\text{Fe})$, this dynamic average is in reasonable agreement with experiment, deviating by less than 200 ppm. No persistent "hydridic shift" is computed for the extra proton, and its mean $\delta(^{1}\text{H})$ value is found ca. 4.5 ppm too strongly deshielded with respect to experiment. The ^{1}H(Fe) chemical shift is calculated upfield from the ^{1}H(Cp) resonances, however, at least qualitatively consistent with experiment.

It is conceivable that the accord between theory and experiment would improve with a density functional that preserves a significant population of **2b** and, on average, maintains a closer interaction between iron and the proton in an MD simulation. In any event, dynamically averaged chemical shifts can be quite

(56) The same observation is made for the ^{1}H(Fe) shieldings (not shown).

(57) It should be kept in mind that, due to the limited number of snapshots, the statistical confidence level of the quantitative data is not very high (also reflected in the notable uncertainty of the averaged shieldings mentioned in the computational details); the qualitative results, however, should be reliable, in particular when discussing deviations from experiment on the order of 1600−2300 ppm, as in the case of the BOMD/B3LYP simulations.

sensitive to details of the MD, making such computations of the NMR parameters a sensitive probe not only for the accuracy of the underlying equilibrium geometry but also for the quality of the PES in its vicinity.[58]

As is well known, the classical propagation in the MD simulations does not take the quantum nature of the nuclei into account and neglects possible quantum effects on their mobility. This shortcoming should be particularly important for the lightest nuclei, such as the critical proton in our case. These effects can be described by solving the nuclear Schrödinger equation,[59] which is only feasible for very small systems, or by suitable quantum dynamical approaches, for instance based on Monte Carlo[60] or Path-Integral CPMD methods.[61] The exceptional mobility of a proton in water has been studied using the latter approach,[62] and it has been concluded that in this case quantum effects are important, but do not alter the basic qualitative aspects of the transport mechanism.[63] Similar simulations would be desirable for **2**, but are a formidable task, due to the complexity of the system and its sensitivity toward the computational details that define the PES.

As a first step toward a study of quantum effects, we have assessed zero-point corrections on the chemical shifts, using a perturbational approach that was recently introduced[7] and tested for a large set of transition metal complexes.[6,8] The results are included in Table 4, where δ_{eff} denotes a single, static computation for an effective geometry obtained from vibrational averaging over the zero-point motion, and δ_0 includes, on top of that, the effects of the curvature of the magnetic shielding hypersurface around this effective geometry. As noted before for transition metal chemical shifts,[6] the main change from the equilibrium value δ_e is contained in δ_{eff}, and only relatively minor further changes arise on going from δ_{eff} to δ_0. We will discuss only δ_0 values in the following.

For **1** and **2a**, the zero-point correction and the classical thermal effect as assessed by MD are qualitatively very similar. Both lead to a deshielding of the ^{57}Fe and ^{1}H(Fe) nuclei and to an upfield shift of the Cp resonances (compare, e.g., BP86/AE1(*) δ_e in normal face versus the corresponding δ_0 in italics and CP-opt versus CPMD entries in Table 4). Quantitatively, the zero-point effects are smaller than those due to classical thermal averaging. For instance, for $\delta(^{57}\text{Fe})$ the latter are about twice as large (ca. 200 ppm) as the former (ca. 100 ppm), for both **1** and **2a**, consistent with previous results for transition metal chemical shifts in general.[6]

It should be kept in mind that both approaches, quantum-mechanical zero-point corrections and MD-based thermal averaging, describe very different things and that it is not possible to simply use the computed changes in δ as increments and add them up. However, since both effects have the same physical origin, namely, the anharmonicity of the PES and the curvature of the magnetic shielding hypersurface, it is sensible to discuss them together.

Larger zero-point effects are obtained for **2b** at the BP86/AE1(*) level: the ^{57}Fe and ^{1}H(Fe) chemical shifts increase by ca. 700 and 6 ppm, respectively, with respect to δ_e, and the δ_0 values closely approach those of symmetric **2a**. In fact, the effective geometry computed for **2b** is also similar to that of **2a**, with a much more symmetric location of the proton between both Cp rings than in the equilibrium geometry. On going from r_e to r_{eff}, the C···H distances in **2b** approach each other from 1.403/2.264 Å (Table 3) to 1.827/1.927 Å, the latter being not far from the r_{eff} values in **2a,** 1.874/1.874 Å. Essentially the same is found at the BP86/SVP level, where again structural characteristics and NMR properties of **2b** change toward those of **2a** upon vibrational averaging (see Table 4). Certainly these results should be taken with a grain of salt, since it is not clear to what extent the perturbational approach and the truncated expansion of the vibrational wave function are applicable in this case. If this approach is valid, these results indicate that even if the BP86/AE1(*) and BP86/SVP PESs with the shallow minimum for **2b** would be correct, this minimum would not be stable at 0 K, where only **2a** would be found. The concomitant prediction that, thus, no "hydridic shift" should be observed in the ^{1}H NMR spectrum at absolute zero is interesting, but extremely difficult to verify. At room temperature, the high mobility of the extra proton should allow for sampling of larger regions of phase space (including regions resembling **2a** and **2b**), a situation that, in the classical limit, is modeled by the MD simulations discussed above. In particular for the BP86/SVP level with its quasi-degenerate shallow minima, these classical thermal fluctuations may well present a more realistic description of the real system at room temperature than that emerging from quantum fluctuations at 0 K.[64]

At the B3LYP/AE1(*) level, zero-point corrections produce no qualitative changes for the chemical shifts of **2a** and **2b** (compare δ_e and δ_0 values in normal face and in italics, respectively, in Table 4). In particular, the characteristics of the symmetric minimum **2a** are unaltered,[65] in contrast to the MD simulation, which collapsed to the more stable agostic form, **2b**. Interestingly, for **2b** the zero-point motion causes an upfield shift of the ^{57}Fe resonance, by ca. 100 ppm (compare B3LYP/ AE1(*) δ_e and δ_0 entries in Table 4), whereas zero-point corrections typically serve to deshield the

(58) In this paper we have not performed extensive basis set tests. While it would be desirable to calculate the properties for each functional at the basis-set limit (as one referee suggested), this would be extremely demanding for the MD-derived thermal averages of this study; moreover, it is unlikely that the qualitative conclusions would be affected (see footnote 44 and compare B3LYP/AE1 and B3LYP/TZVP(+) entries in Table 4).

(59) See for instance: Sundholm, D.; Gauss, J.; Schäfer, A. *J. Chem. Phys*. **1996**, *105*, 11051−11059.

(60) Böhm, M. C.; Schulte, J.; Ramírez, R. *Int. J. Quantum Chem*. **2002**, *86*, 280−296.

(61) (a) Marx, D.; Parrinello, M. *Z. Phys. B* **1994**, *95*, 143−144. (b) Tuckerman, M. E.; Marx, D.; Klein, M. L.; Parrinello, M. *J. Chem. Phys*. **1996**, *104*, 5579−5588.

(62) Marx, D.; Tuckerman, M. E.; Hutter, J.; Parrinello, M. *Nature* **1999**, *397*, 601−604.

(63) Tuckerman, M.; Laasonen, K.; Sprik, M.; Parrinello, M. *J. Chem. Phys*. **1995**, *103*, 150−161.

(64) In principle, the perturbational approach for zero-point corrections can be extended to evaluate effective geometries and averaged properties at thermal equilibrium for a given temperature (see e.g.: Ruden, T. A.; Ruud, K. In *Calculation of NMR and ESR Parameters. Theory and Applications*; Kaupp, M., Bühl, M., Malkin, V. G., Eds.; Wiley-VCH: Weinheim, 2004; pp 153−173). To our knowledge, however, systematic tests and benchmarks for this method have not yet been reported.

(65) Note that symmetry is not exploited in our implementation of the vibrational corrections, so that in principle effective geometries with lower symmetries could be formed.

metal. Thus, in the case of **2b** the error in $\delta(^{57}Fe)$ with respect to experiment is somewhat reduced on going from δ_e to δ_0, but both miss the observed value by a wide margin. In summary, the B3LYP zero-point corrections reinforce the conclusion drawn from the static and MD results, namely, that experimental $\delta(^{57}Fe)$ and $\delta(^{1}H)$ values are best reconciled with **2a** and **2b**, respectively.

Finally, the neglect of solvent and counterions in the computations deserves some comments. The ^{57}Fe and ^{1}H NMR spectra have been recorded in aqueous BF_3,[12b] which is also the protonating agent, producing $[BF_3(OH)]^-$ as counterions. In light of the sensitivity of structures, energetics, and chemical shifts of **2a** and **2b** on the computational setup, it might be expected that interactions with the solvent and/or the counterions could be just as important for these observables. However, the ^{1}H chemical shifts of **2** stay almost the same upon switching from aqueous BF_3 to superacid as reaction medium,[12b,13] suggesting that the basic structure of **2** is not sensitive to the particular solvent. In the gas phase, relatively weak interactions between **2** and single, otherwise strongly donating solvent molecules such as acetonitrile have been noted.[14] Likewise, the counterions present in superacid, typically SbF_6^- or $Sb_2F_{11}^-$, are only weakly coordinating, so that no important interaction between them and the title cation is to be expected. Even though of notable polarity, this medium does not seem to affect chemical shifts of solutes significantly, as the vast majority of chemical shifts of carbocations, measured in superacid, are well described computationally for the isolated species.[66] In a few test calculations in which **2a** and **2b** were embedded in a polarizable continuum, no significant effect of the dielectric constant of the surrounding medium on the relative energies and chemical shifts was found. We are thus confident that the results presented in Table 4 and discussed above are not artifacts of the gas-phase conditions adopted in the computations and that our conclusions are meaningful also for the actual system in solution.

Conclusions

The fluxional character of neutral and protonated ferrocene has been studied computationally, calling special attention to explicit molecular dynamics simulations on quantum-mechanically derived potential energy surfaces. For neutral ferrocene (**1**), the course of the simulation can depend on the starting conditions, and either the molecule may fluctuate within a single potential well, or the two Cp rings may rotate freely and unhindered with respect to each other. The radial distribution curve derived from the single-well simulation fits better to experiment (GED) than that from the freely rotating model.

Protonated ferrocene turns out to be a problem case for density functional methods, as the structures and relative energies of the two relevant minima, described as metal-protonated (**2a**) and ring-protonated (or agostic, **2b**), can depend very sensitively on subtle computational details, such as exchange−correlation functional or basis set. In such a case it is difficult to obtain conclusive results, and care should be taken when interpreting data from just one theoretical level. As a consequence of these results, the MD simulations can follow quite different routes on different PESs. The system can stay predominantly in regions resembling **2a**, as in CPMD simulations with the BP86 functional, it can mainly sample regions corresponding to **2b**, as in BOMD/B3LYP simulations, or both forms can be populated to a similar extent, as in BOMD simulations at the BP86/SVP level. These simulations have in common that the extra proton is highly mobile and can migrate quickly around the perimeter and from agostic contacts with one carbon to another. At the same time, rotation of the two Cp rings relative to each other is facile and occurs on the picosecond time scale. Thus, a quite detailed qualitative picture of the fluxional processes emerges from these simulations, even if aspects such as actual rates or relative populations are difficult to quantify. These findings are fully consistent with the observed equivalence of all ^{13}C and ^{1}H resonances of the Cp rings on the NMR time scale. From static equilibrium chemical shifts, from thermal averages over the MD trajectories, and from quantum-mechanical zero-point corrections it appears that the experimental $\delta(^{57}Fe)$ value is best reproduced by symmetrical structures resembling **2a**, whereas the ^{1}H NMR spectrum is better reconciled with an agostic structure **2b**. So far, none of the static or dynamic models can quantitatively reproduce both sets of NMR data at the same time. In a more qualitative sense, a reasonable accord between experiment and theory is found at the BP86/SVP level, both for the equilibrium value of the agostic minimum **2b** and for the dynamic average during the MD simulations that sample both **2a** and **2b**. The latter simulations are thus indicated to offer a faithful description of the fluxional character of **2**.

An important result is that there can be noticeable differences when molecular properties (chemical shifts in our case) are averaged over trajectories within one potential well, or when they are sampled over "reactive" parts of the PES, such as Cp rotation or proton migration. Assessment of such fluxional motions by chemical shift calculations can be seen as a new area of application of computational NMR spectroscopy (assuming that agreement between observed and modeled δ values can be achieved only if both the equilibrium geometries and the dynamical processes involved are accurately described by the computations). This methodology provides a stringent test for the quality of the underlying PES, a test that DFT methods have yet to pass for **2**. As far as the structure and dynamics of protonated ferrocene are concerned, the final word[17] has yet to be spoken.

Acknowledgment. M.B. wishes to thank Prof. W. Thiel and the Deutsche Forschungsgemeinschaft for continuing support. We thank Dr. Petra Imhof for assistance with her vibrational averaging program. Computations were performed on Compaq XP1000 and ES40 workstations as well as on an Intel Xeon PC cluster at the MPI Mülheim, and on a Hitachi SR-8000 supercomputer at the Leibniz Rechenzentrum in Munich.

OM049243G

(66) See for instance: Siehl, H. U.; Vrček, V. In *Calculation of NMR and ESR Parameters. Theory and Applications*; Kaupp, M., Bühl, M., Malkin, V. G., Eds.; Wiley-VCH: Weinheim, 2004; pp 371−394.